

RESEARCH ARTICLE

Radar-based heavy precipitation events in Germany and associated circulation patterns

Angelika Palarz  | Paul James | Thomas Junghänel | Jennifer Ostermüller |
Ewelina Walawender  | Thomas Deutschländer

Deutscher Wetterdienst, Offenbach am Main, Germany

Correspondence

Angelika Palarz, Deutscher Wetterdienst, Frankfurter Strasse 135, 63067 Offenbach am Main, Germany.

Email: angelika.palarz@dwd.de

Funding information

Federal Ministry for Digital and Transport (BMDV)

Abstract

As projected by multiple climate models, short-duration heavy precipitation events (SDHPEs) are expected to intensify particularly quickly under the changing climate posing substantial risk to natural and human systems. Yet over the years, SDHPEs have received less scientific attention than long-duration heavy precipitation events (LDHPEs), mainly due to the limitations of measurement systems. Our aim is to provide insight into spatial and temporal variability of SDHPEs detected by the radar network of the *Deutscher Wetterdienst* (DWD) in Germany from 2001 to 2020 as well as to explore their links to circulation patterns (CPs). The study is based on the Catalogue of Radar-based heavy Rainfall Events (CatRaRE) generated using reprocessed gauge-adjusted data of the DWD radar network as well as a new numerical method for classifying CPs over Central Europe called “*Großwetterlagen* for Reanalyses” (GWL-REA). The results have demonstrated that SDHPEs, which are defined based on either locally valid precipitation values with a return period of 5 years (CatRaRE T5) or absolute precipitation values equal to DWD Warning Level 3 (CatRaRE W3), are common phenomena occurring most frequently in the afternoon hours of the summer season. They constitute up to 90% of all heavy precipitation events included in the catalogues covering relatively small areas—the median area of SDHPEs ranges from 22 km² (CatRaRE T5) to 24 km² (CatRaRE W3), while the median area of LDHPEs ranges from 175 km² (CatRaRE W3) to 184 km² (CatRaRE T5). As compared to LDHPEs, SDHPEs are generated by a wider spectrum of circulation conditions, including not only cyclonic but also anticyclonic CPs. In the warm season, the anticyclonic CPs, often accompanied by air mass advection from the south, can induce high thermal instability leading to the development of relatively small, isolated convective cells, which often cannot be captured by rain gauge stations.

KEYWORDS

CatRaRE, circulation patterns, GWL-REA, heavy precipitation events, long-duration precipitation, radar data, short-duration precipitation

This is an open access article under the terms of the [Creative Commons Attribution](https://creativecommons.org/licenses/by/4.0/) License, which permits use, distribution and reproduction in any medium, provided the original work is properly cited.

© 2023 The Authors. *International Journal of Climatology* published by John Wiley & Sons Ltd on behalf of Royal Meteorological Society.

1 | INTRODUCTION

Increasing concentration of water vapour in the Earth's atmosphere being a result of continued global warming has a pronounced impact on precipitation patterns. Numerous studies have reported that particularly affected are heavy precipitation events (HPEs), the frequency and intensity of which have risen over the last few decades in many regions of the world (Li, Xuan, et al., 2018b; Iqbal et al., 2019; Powell & Keim, 2015; Ryan et al., 2021). As projected by multiple climate models, this tendency will continue or even accelerate by the end of the 21st century (Donat et al., 2019; Li, Chen, et al., 2018a; Rajczak & Schär, 2017; Supari et al., 2020). On the global scale, HPEs are expected to intensify at a rate of 6%–7% per each 1°C of air temperature warming following the Clausius–Clapeyron (CC) relationship (IPCC, 2023). However, many regional studies have already shown that the CC rate is more appropriate for long-duration heavy precipitation events (LDHPEs; daily to multiday events) than for short-duration heavy precipitation events (SDHPEs; hourly to subdaily events), which may increase at twice the rate expected from the CC relationship (Ali et al., 2021; Ali et al., 2022; Ban et al., 2015; Fowler et al., 2021; Lenderink & Meijgaard, 2008; Loriaux et al., 2013).

The observed and projected changes in precipitation patterns pose substantial risk to natural and human systems causing more frequent occurrence of flash floods, landslides and soil erosion as well as leading to economic and life losses (IPCC, 2012). It has been projected that population exposure to HPEs and their secondary effects will continue to increase (Chen & Sun, 2021; Liu et al., 2020). On the local scale, the highest population exposure is expected to occur over urban areas, which are particularly vulnerable to SDHPEs due to the design of drainage infrastructure (Chen et al., 2020). As the urban runoff processes occur rather on the time scales of minutes to hours, the hourly to subdaily precipitation events are far more relevant for drainage infrastructure than the daily to multiday precipitation events (Arnbjerg-Nielsen et al., 2013; Kang et al., 2016; Kourtis & Tsihrintzis, 2021; Zhou, 2014). Furthermore, knowledge on SDHPEs is highly needed for (1) modelling of flash floods, debris flows and landslides (Luino et al., 2019; Nguyen et al., 2016; Šálek et al., 2006; Yang et al., 2020); (2) nowcasting applications (Panziera et al., 2016; Romang et al., 2011; Spyrou et al., 2020; Zhai et al., 2018) and (3) validation of high-resolution climate simulations (Blenkinsop et al., 2018; Chan et al., 2020; Kendon et al., 2018; Yun et al., 2020).

While many papers have already focused on LDHPEs properties, comprehensive studies on SDHPEs are still

lacking in the scientific literature. This is mainly due to the limited availability of long-term time series of hourly to subdaily precipitation data. To address this limitation, tremendous efforts have been undertaken in the framework of the European Research Council-funded project “Intelligent use of climate models for adaptation to non-stationary hydrological extremes” (INTENSE), within which subdaily rain gauge precipitation data from across the globe have been collected to form the Global Sub-Daily Rainfall Dataset (GSDR; Blenkinsop et al., 2018; Lewis et al., 2019). However, SDHPEs often cannot be captured by measurements of rain gauge stations, thus requiring an application of spatially contiguous observations of radar networks (Saltikoff et al., 2019; Tapiador et al., 2012). As stated by Lengfeld et al. (2020), only 17.3% of hourly HPEs and 81.8% of daily HPEs detected by the radar network of the *Deutscher Wetterdienst* (DWD) from 2001 to 2018 were captured by rain gauge stations as well. As a rule, the detectability of precipitation events by rain gauge stations decreases strongly with a decreasing duration (Lengfeld et al., 2019). Unfortunately, application of radar data may be limited as well. In particular, time series of radar observations are an order of magnitude shorter than time series of rain gauge stations, which restricts the research on SDHPEs to relatively short time periods (Barton et al., 2020; Berg et al., 2016; Fairman Jr et al., 2015; Paulat et al., 2008). However, the growing collection of radar data as well as progress in the postprocessing algorithms used for their correction have already enabled the construction of the first radar-based SDHPEs climatologies covering longer, at least 10-years, time periods (Bližňák et al., 2018; Fairman Jr et al., 2017; Kreklow et al., 2020; Panziera et al., 2018).

An important aspect of the research on HPEs is their genesis and links to meso- and macroscale circulation patterns (CPs). Many studies have investigated these links by applying atmospheric circulation indices, such as Arctic Oscillation, El Niño–Southern Oscillation and North Atlantic Oscillation (Dong et al., 2019; Irannezhad et al., 2017; Kenyon & Hegerl, 2010; Merino et al., 2016) or multivariate statistical techniques (Fernández-Montes et al., 2014; Rimbu et al., 2016; Tan et al., 2019; Ullah et al., 2021). Other widely used tools for assessing CPs constitute circulation type classifications, among which probably the best-known is the manual *Großwetterlagen* (GWL) classification given by Hess and Brezowsky (1952). The GWL classification and its numerical versions, for example, objective GWL or SynopVis GWL, have been already successfully applied in studies on CPs associated with daily to multiday HPEs occurring over Central Europe (Brieber & Hoy, 2019; Hoy et al., 2014; Jaagus et al., 2010; Minářová et al., 2017a;

Minářová et al., 2017b; Ustrnul & Czekierda, 2001). To account for mesoscale climate peculiarities, some regional classifications have also been created and implemented in research on LDHPEs (Lupikasza, 2010; Mika et al., 2021; Řehoř et al., 2021; Twardosz & Niedźwiedz, 2001). On the other hand, the genesis of SDHPEs and their links to CPs, although vital, remain largely unstudied.

Therefore, the overarching aim of this study is to gain insight into spatial and temporal variability of SDHPEs detected by the DWD radar network in Germany from 2001 to 2020 as well as to explore their links to CPs expressed in the form of a new GWL-based classification. Our intention is also to present the results in a broader context by comparing properties of SDHPEs and LDHPEs. The paper is structured as follows: section 2 introduces the radar and circulation data as well as outlines the definitions and methods applied; section 3 describes the results obtained; section 4 provides the conclusions and highlights challenges of further research on HPEs.

2 | DATA AND METHODS

2.1 | Radar data

The study is based on the freely-available Catalogue of Radar-based heavy Rainfall Events (CatRaRE) generated using the reprocessed gauge-adjusted data of the DWD radar network known as RADKLIM (Lengfeld et al., 2021b, 2021c; Winterrath et al., 2018). The hourly precipitation fields, available there at the resolution of $1 \text{ km} \times 1 \text{ km}$, have allowed the creation of two versions of the catalogue, both of which contain HPEs of 11 durations (i.e., 1, 2, 3, 4, 6, 9, 12, 18, 24, 48 and 72 h). The two versions differ in terms of the thresholds used to define a heavy precipitation event—CatRaRE T5 applies locally valid, grid-based precipitation values with a return period of 5 years, while CatRaRE W3 applies nationwide absolute values equal to DWD Warning Level 3. Lengfeld et al. (2021a) highlighted that the threshold defined by the return period of 5 years correspond to the minimum requirements for the drainage infrastructure in Germany, while the threshold defined by the DWD Warning Level 3 indicate potentially dangerous precipitation events able to cause both local and widespread regional damages. As shown in Table 1, the threshold applied for detection of the heavy precipitation event in both versions of the catalogue depends on the event duration, while, in CatRaRE T5, it varies also spatially reaching generally higher values in the southern than in the northern Germany.

The identification of HPEs is carried out in two stages. The first stage includes the detection of locally

TABLE 1 Precipitation sum thresholds applied for detection of the heavy precipitation event in CatRaRE T5 and CatRaRE W3 depending on the event duration

Duration (h)	1	2	3	4	6	9	12	18	24	48	72
CatRaRE T5 (mm)	14.8–28.8	18.9–36.5	21.4–42.8	22.4–53.0	26.1–56.0	29.2–65.7	31.6–73.5	35.2–87.3	37.8–99.6	44.4–137.8	48.7–167.6
CatRaRE W3 (mm)	25.0	27.0	29.0	31.0	35.0	37.5	40.0	45.0	50.0	60.0	90.0
Minimum event size (km ²)	9.0	9.0	9.0	12.0	18.0	27.0	36.0	54.0	72.0	144.0	216.0

Note: The last row indicates also the minimum size of the heavy precipitation event depending on the events duration—this value does not differ among CatRaRE versions.

limited contiguous rainfall objects for which the precipitation sums at individual grid cells exceed the threshold defined separately for each time step and event duration. The minimum size of the rain object depends, as defined by Lengfeld et al. (2021a), on the event duration—it is equal to 9 km² for events lasting no more than 3 h and equal to three times the duration for events lasting more than 3 h, for example, 36 km² for an event of 12 h duration (Table 1). Since rainfall can last several hours and exceed the threshold for HPEs for more than one duration (e.g., in the case of 6 h of persistent rain, the threshold for HPEs might not only be exceeded for the 6 h precipitation sum but also for 1, 2, 3 or 4 h precipitation sum), multiple rainfall objects, representing in fact the same event but at different durations, can be detected. Therefore, the second stage aims to ensure the temporal and spatial independence of the rain events. To ensure the temporal independence of two rainfall events that occur in the same area, a minimum time gap between the end of one and the beginning of the next rainfall event is required. This time gap has to be equal or greater than the duration of the shorter event, but not smaller than 4 h. Furthermore, if multiple rain objects are identified in the same time interval, a check for spatial independence is performed—the rain objects that overlap are spatially dependent and described as the same rain event. If multiple rainfall objects are temporally and spatially dependent, the strongest one, according to Extremity Index defined by Müller and Kaspar (2014), is included in the catalogue. The other rain objects are, in turn, neglected and excluded from further investigation. For more detailed information on the process chain leading to the identification of heavy rainfall events, readers are encouraged to seek out the paper of Lengfeld et al. (2021a).

2.2 | Circulation data

As mentioned already, the study applies a new numerical method for classifying CPs over Central Europe called “*Großwetterlagen* for Reanalyses” (GWL-REA), used here for the first time. This method is based on the well-known manual GWL classification given by Hess and Brezowsky (1952), in which 29 GWL types have been classified using historical weather charts back to 1881. As part of the tradition, the manual GWL classification is regularly updated at the DWD, although its major disadvantage remains inhomogeneity resulting from the subjective assessments by various meteorologists. To remove this inhomogeneity, a numerical method for classifying GWL was developed by James (2007), successively improved and used in numerous papers (e.g., Drücke

TABLE 2 Abbreviations, definitions and frequencies of the 29 types included in the GWL-REA classification

Abbreviation	Definition	FQ (%)
01 Wa	Anticyclonic westerly	4.3
02 Wz	Cyclonic westerly	9.5
03 Ws	South-shifted cyclonic westerly	1.8
04 Ww	Angular cyclonic westerly	2.8
05 SWa	Anticyclonic south-westerly	5.1
06 SWz	Cyclonic south-westerly	6.3
07 NWA	Anticyclonic north-westerly	2.9
08 NWz	Cyclonic north-westerly	6.2
09 HM	High over central Europe	4.2
10 BM	Bridge across central Europe	8.6
11 TM	Low over central Europe	1.7
12 Na	Anticyclonic northerly	1.3
13 Nz	Cyclonic northerly	1.3
14 HNa	High Norwegian Sea, anticyclonic	2.0
15 HNz	High Norwegian Sea, cyclonic	2.5
16 HB	High over the British Isles	2.8
17 TrM	Upper Trough over central Europe	5.8
18 NEa	Anticyclonic north-easterly	2.5
19 NEz	Cyclonic north-easterly	1.9
20 HFa	High over Fennoscandia, anticyclonic	2.6
21 HFz	High over Fennoscandia, cyclonic	3.3
22 HNFa	High Norwegian Sea-Fennoscandia, anticyclonic	2.1
23 HNFz	High Norwegian Sea-Fennoscandia, cyclonic	3.0
24 SEa	Anticyclonic south-easterly	2.3
25 SEz	Cyclonic south-easterly	2.1
26 Sa	Anticyclonic southerly	3.2
27 Sz	Cyclonic southerly	1.4
28 TB	Low over the British Isles	2.2
29 TrW	Upper Trough over western Europe	4.2

Note: The frequency of a given type (FQ) has been calculated for the research period 2001–2020 and is expressed here as a percentage value.

et al., 2021; Minářová et al., 2017a, 2017b; Wapler & James, 2015). GWL-REA builds broadly on this previous approach with the aim of further improving its accuracy and efficiency.

GWL-REA is produced using pattern correlations between daily and pre-defined, reference climatological patterns constructed for the Europe–North Atlantic domain. The domain covers an area extending from 20°N to 80°N and from 30°W to 60°E on a 2° × 2°

latitude-longitude grid. The input data consist of mean sea level pressure, 500 hPa geopotential height, 500–1000 hPa relative geopotential thickness and precipitable water column, gained from the reanalysis dataset ECMWF ERA5, which is currently available from 1959 onwards (Hersbach et al., 2020).

Similar to the previous numerical GWL method, reference climatological patterns are required for the pattern correlations. However, while the previous version only used a single pair of seasonally biased reference climatological patterns for each GWL type, the number of the reference climatological patterns distinguished in GWL-REA has been increased to well over 200 in order to account for the within-type variability more effectively, reducing related errors. The resulting large number of correlation coefficients calculated for each daily pattern are then combined onto the 29 GWL types using a many-to-one mapping.

The new method also addresses a specific problem that the daily GWL type obtained from the pattern correlation alone does not always correspond to the specific nomenclature of the given GWL type in terms of the central anticyclonicity (cyclonicity) or location of the steering high (low). A new postprocessing module calculating parameters derived from the Lamb Weather Types method (LWT; Jenkinson & Collinson, 1977) has been implemented to address this issue. The LWT parameters include circularity, cyclonicity, flow direction, flow strength and vorticity to flow gradient ratio calculated over seven regions defined in accordance with GWL nomenclature allowing the initial correlation coefficients of a particular GWL type to be reduced systematically in cases where the daily pattern does not correspond to that expected for the given GWL type, according to its nomenclature.

The resulting time-series is also subjected to temporal filtering, which ensures that an event with a particular circulation pattern lasts at least 2 days. This is shorter than the 3-day minimum event duration specified in the manual GWL given by Hess and Brezowsky (1952), but has the advantage of allowing more short-lived events to remain in the time series, which improves correlations with precipitation statistics, for example.

Nonetheless, the 29-type Hess-Brezowsky GWL system has one specific disadvantage with regards to its application in climatological studies that still needs to be addressed, namely that it concentrates on atmospheric circulation alone and largely ignores air mass properties. Some GWL types have consistent air masses over Central Europe, such as the northerly types, Na, Nz and TrM, which are all cold types (Table 2). However, most of the remaining GWL types can have very different air masses at times, with correspondingly different midtropospheric

TABLE 3 Abbreviations, definitions and frequencies of the 12 circulation-air mass groups included in the GWL-REA_{GROUPS} classification

Abbreviation	Definition	FQ (%)
01 AWm	Anticyclonic, warm, Atlantic-maritime	9.5
02 AWc	Anticyclonic, warm, continental	10.3
03 AGb	Anticyclonic, air mass boundary, blocking high	4.9
04 AGz	Anticyclonic, boundary, zonal circulation	7.8
05 AKm	Anticyclonic, cold, polar(arctic)-maritime	4.3
06 AKc	Anticyclonic, cold, polar-continental	6.6
07 ZWm	Cyclonic, warm, Atlantic-maritime source	11.1
08 ZWc	Cyclonic, warm, Mediterranean source	7.6
09 ZGm	Cyclonic, air mass boundary, maritime	9.5
10 ZGr	Cyclonic, surface frontal trough or warm advection	9.7
11 ZKm	Cyclonic, cold, polar(arctic)-maritime	12.3
12 ZKc	Cyclonic, cold, continental with warm advection	6.4

Note: The frequency of a given group (FQ) has been calculated for the research period 2001–2020 and is expressed here as a percentage value.

structures over the respective characteristic surface flow patterns. As such, the within-type variability of synoptic structures can be quite high for many of the GWL types, reducing their usefulness for studies that depend on air mass properties, especially for temperature, but also for precipitation; the latter depending on moisture content and air mass boundaries as well as on low-level vorticity.

To address this problem, GWL-REA defines a set of GWL subtypes, which separate the distinct air masses more effectively. Each GWL type is divided into between 1 and 4 subtypes, resulting in 60 subtypes in total. The initial GWL classification then spawns a second, more detailed classification of the GWL subtypes, which could be used directly. However, due to the very large total number of subtypes, a more useful final product can be constructed by concatenating the subtypes into 12 basic circulation-air mass groups, separated into two vorticity classes (anticyclonic–cyclonic), three temperature classes (warm–mixed–cold) and two source region or circulation form classes (e.g., maritime-continental, blocked-zonal).

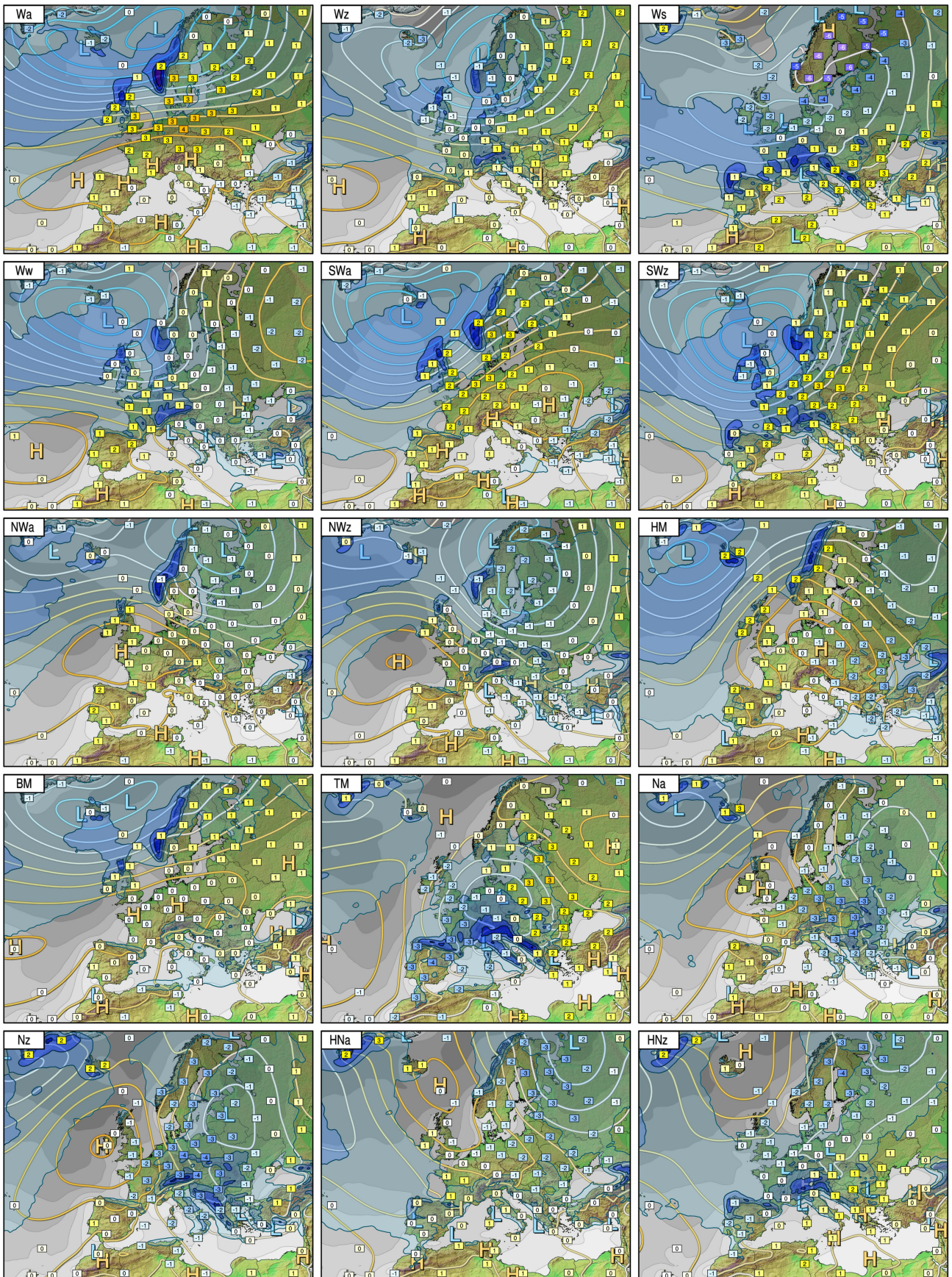


FIGURE 1 Legend on next page.

As a result of this strict grouping of vorticity, temperature and source region classes, this new GWL-derived classification system, referred to as GWL-REA_{GROUPS} and deployed for the first time in this study, is a very effective way of distinguishing between different fundamental synoptic situations, while keeping the total number of CPs relatively small. The definitions and mean frequencies of occurrence of the 29 types and 12 circulation-air mass groups in GWL-REA are listed in Tables 2 and 3, while the reference climatological composites are plotted in Figures 1–3, respectively.

2.3 | Remarks on definition of SDHPEs and LDHPEs

A review of scientific literature reveals that the definitions of short- and long-duration precipitation events varies. The subdivision of temporal and spatial scales for atmospheric processes given by Orlanski (1975) assumes that, for example, thunderstorms last up to a few hours covering areas of tens of kilometres, while frontal systems may last more than a day covering areas of hundreds of kilometres. Following this approach, there is also a general consensus that SDHPEs occur on a time scale of several minutes to hours, while LDHPEs occur rather on a time scale of several hours to days. However, the exact distinction between SDHPEs and LDHPEs often remains unclear. For instance, Bližňák et al. (2018) defined SDHPEs as events lasting up to 6 h, Lengfeld et al. (2021a) as events lasting up to 9 h, while Oh and Sushama (2020) as events lasting up to 12 h. To maintain the comparability of our research with previous studies conducted on the basis of the DWD radar network data, we have applied the definitions introduced by Lengfeld et al. (2021a)—SDHPEs are defined as events that last 1–9 h, while LDHPEs are defined as events that last 12–72 h.

2.4 | Statistical methods

To gain insight into nature of HPEs, we have computed percentages of the number of HPEs and the area affected by HPEs for each event duration as well as examined the spatial and temporal variability of SDHPEs and LDHPEs. Furthermore, to explore the links between HPEs and

CPs, three indices have been defined, namely (1) probability of the occurrence of a particular circulation pattern given the occurrence of a heavy precipitation event, hereafter $P(\text{CP}|\text{HPE})$; (2) probability of the occurrence of a particular circulation pattern given the occurrence of a day with heavy precipitation event, hereafter $P(\text{CP}|\text{DD}_{\text{HPE}})$ and (3) probability of the occurrence of a day with heavy precipitation event given the occurrence of a particular circulation pattern, hereafter $P(\text{DD}_{\text{HPE}}|\text{CP})$. These indices may be expressed by following formulas:

$$P(\text{CP} | \text{HPE}) = \frac{P(\text{CP} \cap \text{HPE})}{P(\text{HPE})} \times 100\%, \quad (1)$$

$$P(\text{CP} | \text{DD}_{\text{HPE}}) = \frac{P(\text{CP} \cap \text{DD}_{\text{HPE}})}{P(\text{DD}_{\text{HPE}})} \times 100\%, \quad (2)$$

$$P(\text{DD}_{\text{HPE}} | \text{CP}) = \frac{P(\text{CP} \cap \text{DD}_{\text{HPE}})}{P(\text{CP})} \times 100\%, \quad (3)$$

where $P(\text{CP} \cap \text{HPE})$ is the total number of cases for which a particular circulation pattern occurred simultaneously with HPEs, $P(\text{CP} \cap \text{DD}_{\text{HPE}})$ is the total number of days on which a particular circulation pattern occurred simultaneously with a day with HPEs, $P(\text{HPE})$ is the total number of HPEs included in the given CatRaRE version, $P(\text{DD}_{\text{HPE}})$ is the total number of days with HPEs included in the given CatRaRE version and $P(\text{CP})$ is the total number of days with a particular circulation pattern in the years 2001–2020.

To simplify, $P(\text{CP}|\text{HPE})$ shows how often HPEs are accompanied by a particular circulation pattern, $P(\text{CP}|\text{DD}_{\text{HPE}})$ shows how often days with HPEs are accompanied by a particular circulation pattern, and $P(\text{DD}_{\text{HPE}}|\text{CP})$ shows how often a particular circulation pattern leads to a day with HPEs. The $P(\text{CP}|\text{HPE})$ values have been calculated separately for SDHPEs and LDHPEs, while $P(\text{CP}|\text{DD}_{\text{HPE}})$ and $P(\text{DD}_{\text{HPE}}|\text{CP})$ values have been calculated for (1) days on which only SDHPEs occurred ($\text{DD}_{\text{SDHPEs}}$); (2) days on which only LDHPEs occurred ($\text{DD}_{\text{LDHPEs}}$) and (3) days on which both HPEs types, that is, SDHPEs and LDHPEs, occurred ($\text{DD}_{\text{BothHPEs}}$). The distinction between $P(\text{CP}|\text{HPE})$ and $P(\text{CP}|\text{DD}_{\text{HPE}})$ has been introduced to account for the influence of HPEs occurring on the same day. Individual days with a large number of HPEs can skew the results on

FIGURE 1 Reference climatological patterns of types 1–15 included in the GWL-REA classification, showing annual means of daily precipitation (blue filled contours at 2, 4, 6, 10 and 16 mm·day⁻¹), 2 m temperature anomaly (boxes, °C), total cloud coverage (grey background shading, shown here qualitatively) and mean sea level pressure contours (light blue tinge for lower values, yellow-orange tinge for higher values, with high (H) and low (L) centre labels, shown qualitatively). The maps have been generated based on data gained from the reanalysis dataset ECMWF ERA5 [Colour figure can be viewed at wileyonlinelibrary.com]

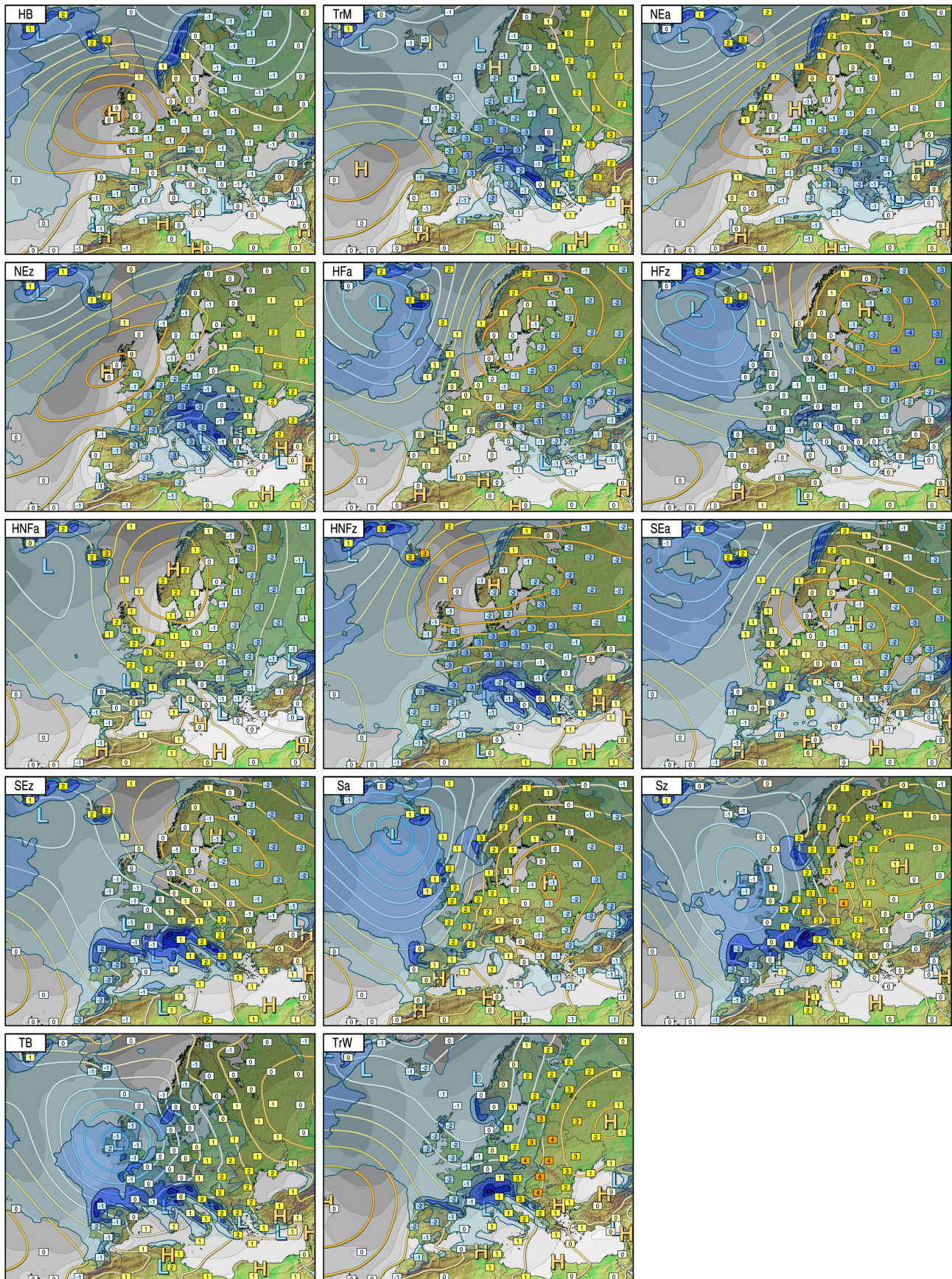


FIGURE 2 As Figure 1, but for types 16–29 included in the GWL-REA classification [Colour figure can be viewed at wileyonlinelibrary.com]

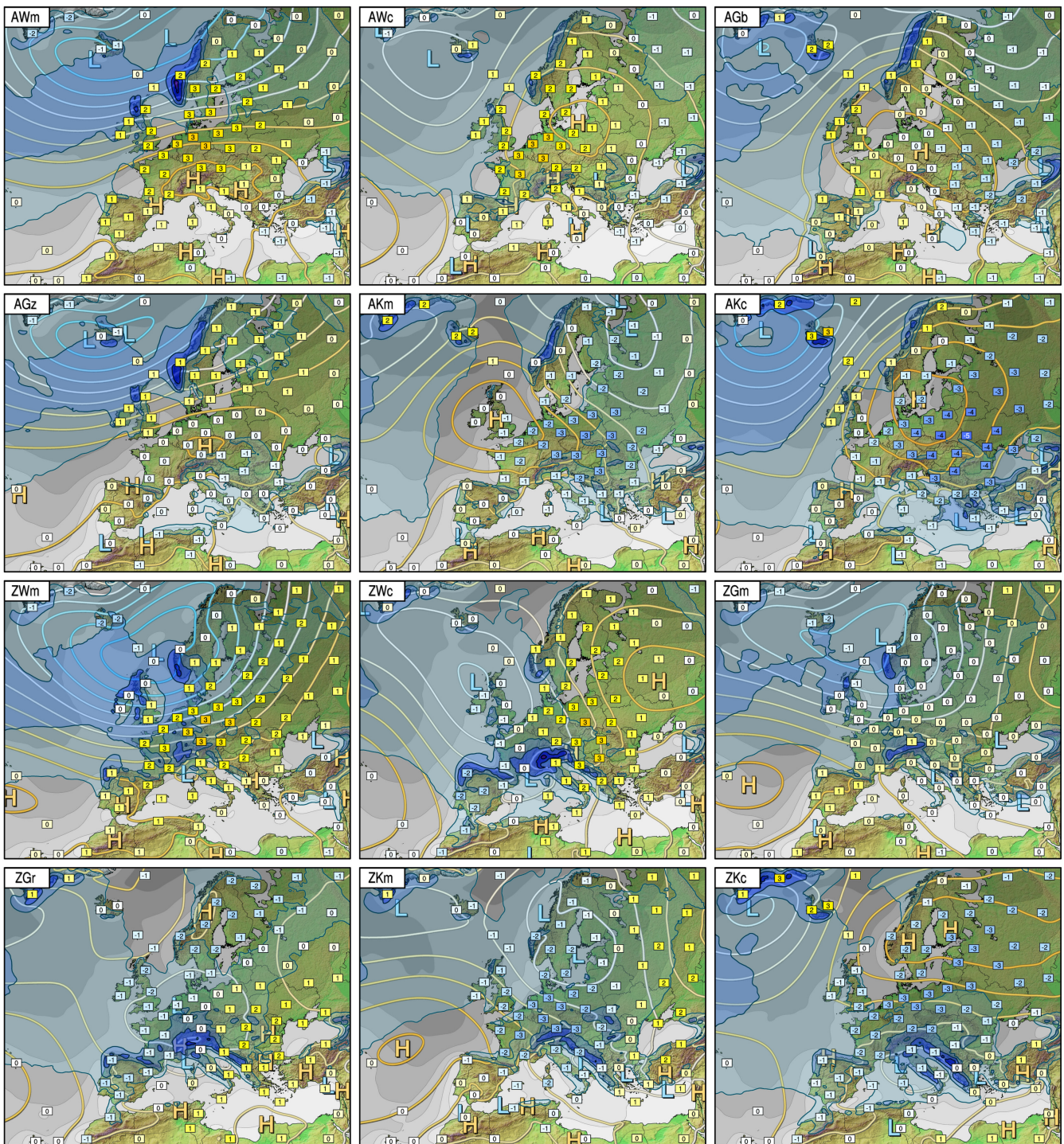


FIGURE 3 As Figure 1, but for circulation-air mass groups 1–12 included in the $\text{GWL-REA}_{\text{GROUPS}}$ classification [Colour figure can be viewed at wileyonlinelibrary.com]

$P(\text{CP}|\text{HPE})$ by overestimating the role of the circulation pattern occurring on such days. As shown in Figure 4, this can be particularly true for SDHPEs—the number of SDHPEs occurring on the same day (either on $\text{DD}_{\text{SDHPES}}$ or $\text{DD}_{\text{BothHPES}}$) relatively often exceeds 100, while the number of LDHPEs occurring on the same day (either on $\text{DD}_{\text{LDHPES}}$ or $\text{DD}_{\text{BothHPES}}$) barely

reaches 25. It should be also noted that all indices have been computed for a circulation pattern occurring at the beginning of a respective heavy precipitation event, although CPs may change in the course of the event. Obviously, this is much less common for SDHPEs than for LDHPES. As an example, CPs change in around 9% of HPEs with duration of 6 h and in around 70%–90% of HPEs with duration of 72 h.

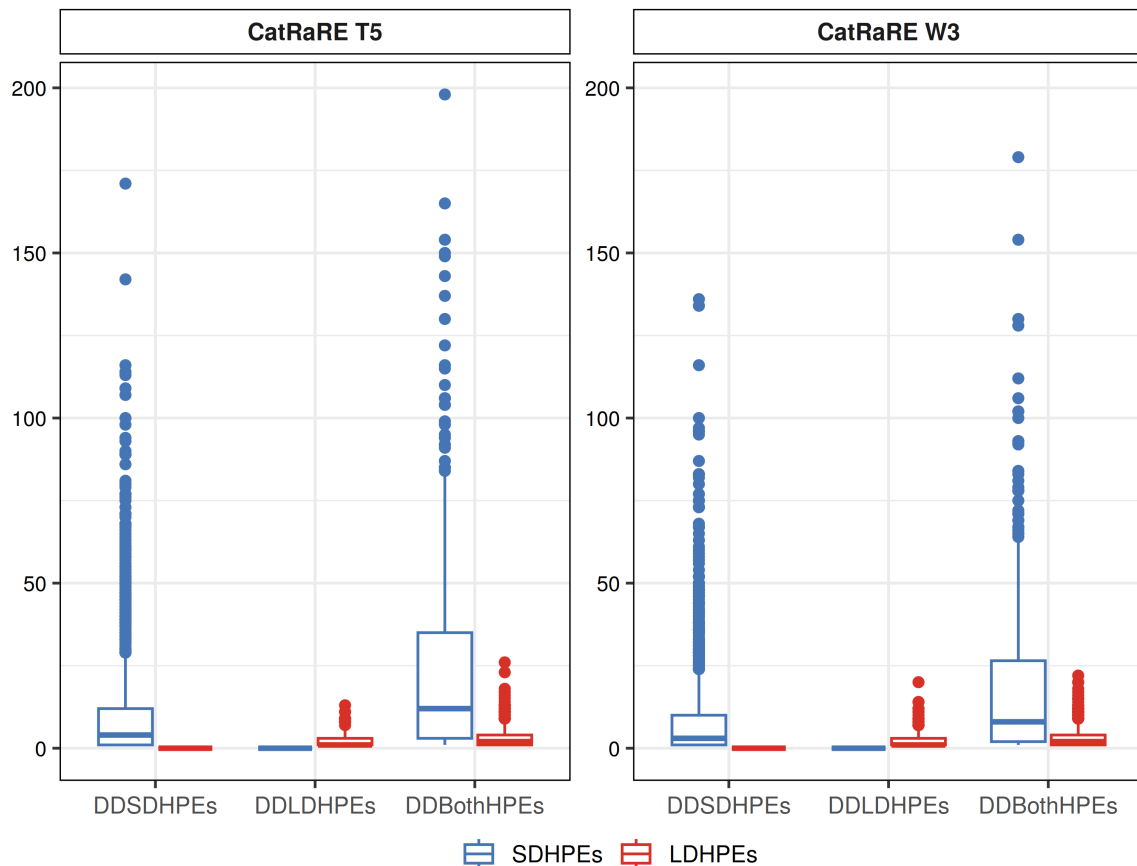


FIGURE 4 Variability in the number of SDHPEs and LDHPEs occurring simultaneously on DD_{SDHPEs} , DD_{LDHPEs} and $DD_{BothHPEs}$ for CatRaRE T5 (left) and CaRaRE W3 (right) in the years 2001–2020. The boxplots visualize the following summary statistics: the box hinges correspond to the first and third quartiles (Q_{25th} , Q_{75th}) showing also the interquartile range ($IQR = Q_{75th} - Q_{25th}$), the central solid line through the boxes indicates the median (Q_{50th}), the upper whisker extends from the Q_{75th} to the largest value no further than $1.5 \times IQR$ from the hinge, and the lower whisker extends from the hinge to the smallest value at most $1.5 \times IQR$. Data beyond the end of the whiskers are plotted individually (blue or red dots) [Colour figure can be viewed at wileyonlinelibrary.com]

For brevity, in the main part of the paper, we present only CPs associated with HPEs included in CatRaRE T5, while the results obtained for HPEs included in CatRaRE W3 are provided in Figures S2 and S3, Supporting Information.

3 | RESULTS

3.1 | HPEs: Spatial and temporal variability

In total, CatRaRE T5 contains 26,881 HPEs and CatRaRE W3 contains 23,020 HPEs. The vast majority of them, up to 90%, constitute SDHPEs. However, the percentage of the total area affected by SDHPEs varies from 35.0% to 41.5%, which implies that SDHPEs, although very frequent, constitute relatively small events occurring on a local rather than regional scale—the median area of SDHPEs equals to 22 km^2 in CatRaRE T5 and 24 km^2 in

CatRaRE W3, while the median area of LDHPEs equals to 184 km^2 in CatRaRE T5 and 175 km^2 in CatRaRE W3. As shown in Figure 5, the percentage of the number of HPEs decreases strongly with an increasing duration, while the percentage of the area affected by HPEs increases with an increasing duration. As an example, CatRaRE T5 includes particularly many HPEs with duration of 1 h, which constitute almost 40% of all HPEs, but account for less than 10% of the area affected, while HPEs with duration of 72 h, which constitute less than 1% of all HPEs, account for almost 17% of the area affected. Similar conclusions can be drawn for CatRaRE W3, albeit both the percentage of the number of HPEs and the percentage of the area affected differ slightly among the catalogues. CatRaRE W3 contains, for instance, substantially less HPEs with duration of 1 and 72 h, which account for very similar percentages of area affected by these precipitation types, amounting to about 4%.

As illustrated in Figure 6, the spatial variability of HPEs depends on the catalogue version and definition

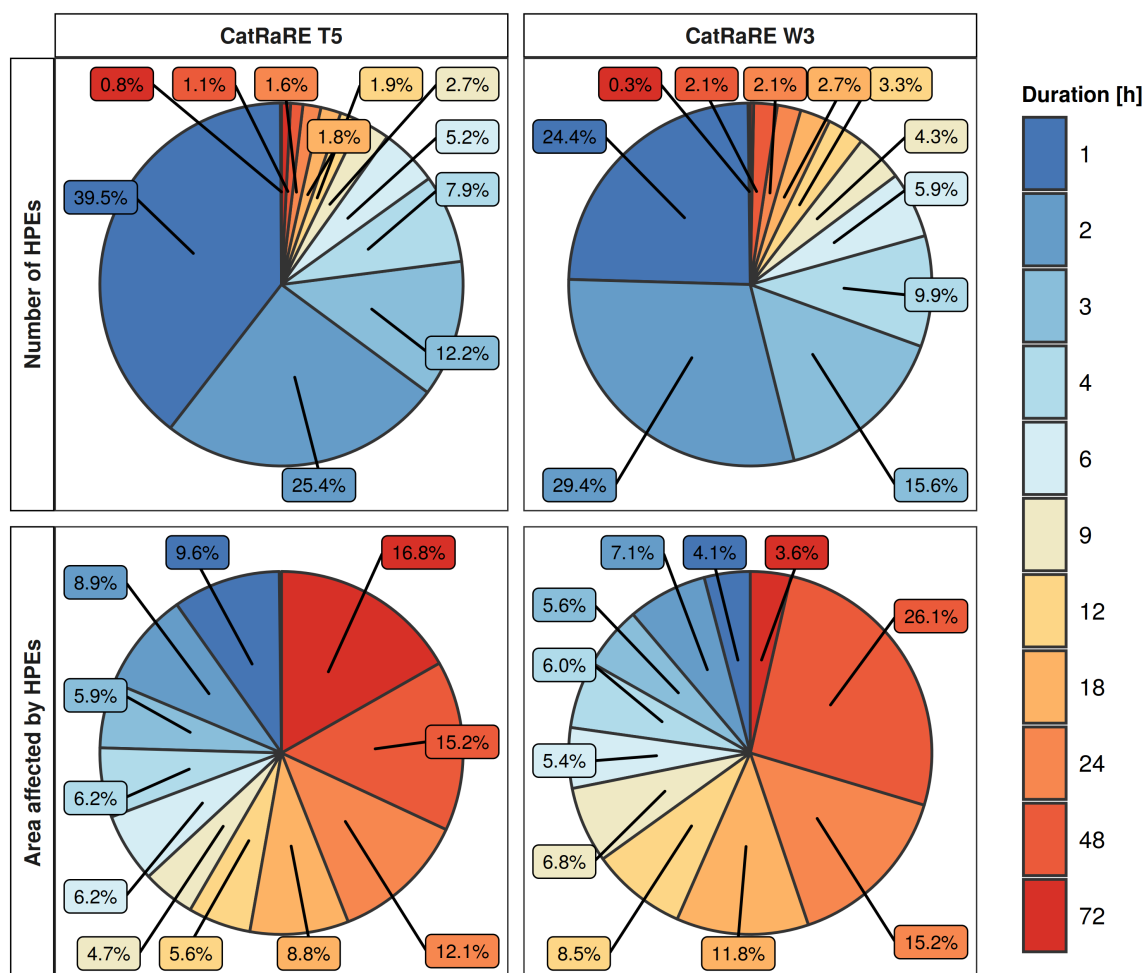


FIGURE 5 Percentage of the number of HPEs (upper row) and percentage of the area affected by HPEs (lower row) depending on the event duration for CatRaRE T5 (left column) and CatRaRE W3 (right column) in the years 2001–2020. The percentage of the number of HPEs of a particular duration has been calculated as a ratio between the total number of HPEs of a particular duration and the total number of all HPEs included in the given version of CatRaRE, while the percentage of the area affected by HPEs of a particular duration has been calculated as a ratio between the total area covered by HPEs of a particular duration and the total area covered by all HPEs included in the given version of CatRaRE [Colour figure can be viewed at wileyonlinelibrary.com]

of HPEs applied therein. CatRaRE T5, which applies locally valid precipitation values with a return period of 5 years, indicates rather homogeneous distribution of both SDHPEs and LDHPEs, while CatRaRE W3, which applies absolute precipitation values equal to DWD Warning Level 3, reflects a general distribution of precipitation over Germany reaching higher values over the high-altitude areas for both SDHPEs and LDHPEs. While LDHPEs included in CatRaRE W3 reach substantially higher number of their occurrence in the mountain areas, for example, in the Alps, Alpine Foothill, Black Forest (located in the western part of the Southwestern Uplands) and Upper Palatine-Bavarian Forest (located in the southern part of the Eastern Uplands), SDHPEs included in CatRaRE W3 are characterized by a slightly higher number of their occurrence only on the border between the Alps and Alpine Foothills. This suggests that

orographic enhancement plays far more important role for LDHPEs than SDHPEs. In particular, as stated by Lengfeld et al. (2019), HPEs with duration of 1–4 h occur in Germany in very similar frequency and intensity over flatlands and mountains. Note also that the higher numbers of LDHPEs per single 1 km × 1 km grid point shown in Figure 6 results rather from the size of LDHPEs than their frequency—an individual long-duration precipitation event covers, on average, much more grid points than short-duration precipitation event. In other words, as LDHPEs cover larger areas, the probability that LDHPEs hits a grid point is much higher. Furthermore, as depicted in Figure 7, SDHPEs are subjected to clear annual and diurnal variability. They occur almost exclusively from April to September and tend to begin between 1200 and 1800 UTC, which along with their reduced sizes, suggests that SDHPEs represent small-scale convective

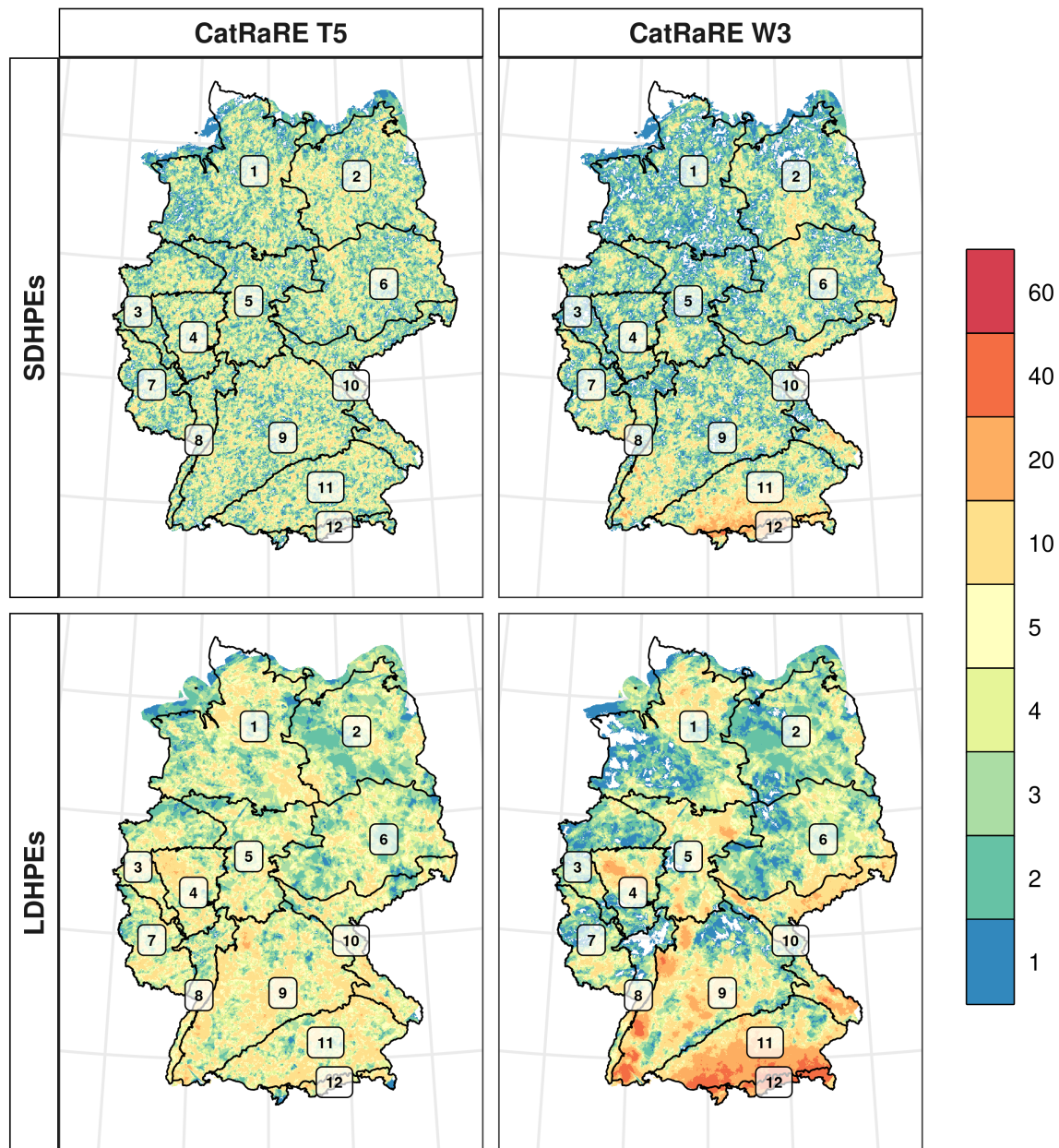


FIGURE 6 Spatial variability of the number of SDHPes (upper row) and LDHPes (lower row) per $1 \text{ km} \times 1 \text{ km}$ grid point for CatRaRE T5 (left) and CatRaRE W3 (right) in the years 2001–2020. The black borders and numbers represent natural regions in Germany, based on the classification of Meynen and Schmithausen (1959): (1) Northwestern Lowlands, (2) Northeastern Lowlands, (3) Western Lowlands, (4) Uplands east of the Rhine, (5) Central Uplands and Harz, (6) Eastern Valleys and Hills, (7) Uplands west of the Rhine, (8) Upper Rhine Lowlands, (9) Southwestern Uplands, (10) Eastern Uplands, (11) Alpine Foothills, (12) Alps [Colour figure can be viewed at wileyonlinelibrary.com]

cells developing under the conditions of high thermal instability. As a contrast, LDHPes occur all year round, also reaching a higher frequency from April to September. Relatively often SDHPes and LDHPes develop simultaneously, occurring on the same day in more or less distant locations— DD_{BothHPEs} constitute from 22.5% (CatRaRE T5) to 26.3% (CatRaRE W3) of all days included in the given catalogue version. Regardless of the catalogue version, DD_{SDHPes} are more frequent than DD_{LDHPes} ,

consisting of 59.4% (CatRaRE W3) to 66.7% (CatRaRE T5) of all days included in the given catalogue version.

3.2 | HPEs: Links to CPs

In CatRaRE T5, SDHPes are most often accompanied by HNz, BM and HFz, while LDHPes are most often accompanied by TM, Wz and TrW. The respective CPs together

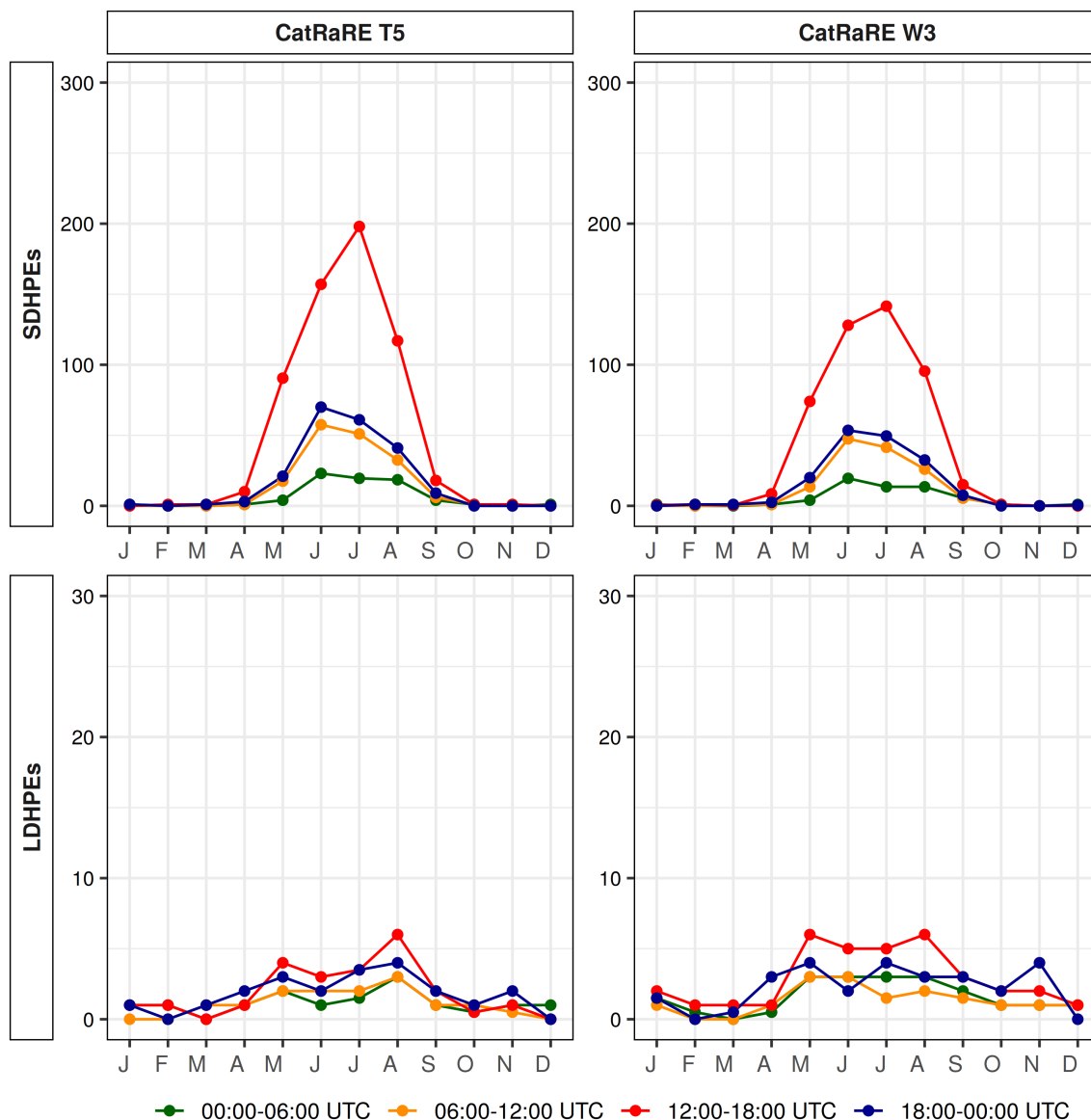


FIGURE 7 Annual and diurnal variability of the median number of SDHPes (upper row) and LDHPes (lower row) for CatRaRE T5 (left column) and CatRaRE W3 (right column) in the years 2001–2020. The colors indicate time of the beginning of HPEs [Colour figure can be viewed at wileyonlinelibrary.com]

account for about 28% of SDHPes and about 40% of LDHPes (Table S1). Overall, in the case of SDHPes, 13 CPs account for at least 75% of their occurrence, while, in the case of LDHPes, 9 CPs account for at least 75% of their occurrence. This suggests that SDHPes are generated by a slightly wider spectrum of circulation conditions, although the results can be partly related to the number of HPEs occurring on the same day, which, as discussed in section 2.4, is usually higher for SDHPes than LDHPes. However, the values of $P(\text{CP}|\text{DD}_{\text{HPE}})$ presented in Figure 8 (left column) lead to similar conclusions—the three most common CPs account for about 26% of all $\text{DD}_{\text{SDHPes}}$ (Wz, BM, TrW) and about 50% of all $\text{DD}_{\text{LDHPes}}$ (Wz, NWz, TrM). For LDHPes, the

pivotal role is played by Wz, which alone accompanies almost one third of $\text{DD}_{\text{LDHPes}}$. Moreover, 75% of all $\text{DD}_{\text{LDHPes}}$ are accompanied by 8 CPs, while 75% of all $\text{DD}_{\text{SDHPes}}$ are accompanied by 15 CPs, half of which constitute anticyclonic CPs, such as BM, Sa, SWa, NEa, HFa, HNFa and HNa. In turn, the cyclonic CPs which often accompany $\text{DD}_{\text{SDHPes}}$, $\text{DD}_{\text{LDHPes}}$ and $\text{DD}_{\text{BothHPEs}}$ are consistent among each other; in particular, there are Wz, NWz, SWz, TrM and TrW. On the other hand, the values of $P(\text{DD}_{\text{HPE}}|\text{CP})$ presented in Figure 8 (right column) indicate that CPs which most often lead to the occurrence of $\text{DD}_{\text{SDHPes}}$ are HNz, HNFa and TrW, while CPs which most often lead to the occurrence of $\text{DD}_{\text{LDHPes}}$ are Wz, Ww and TM. The values of $P(\text{DD}_{\text{HPE}}|\text{CP})$ are, by

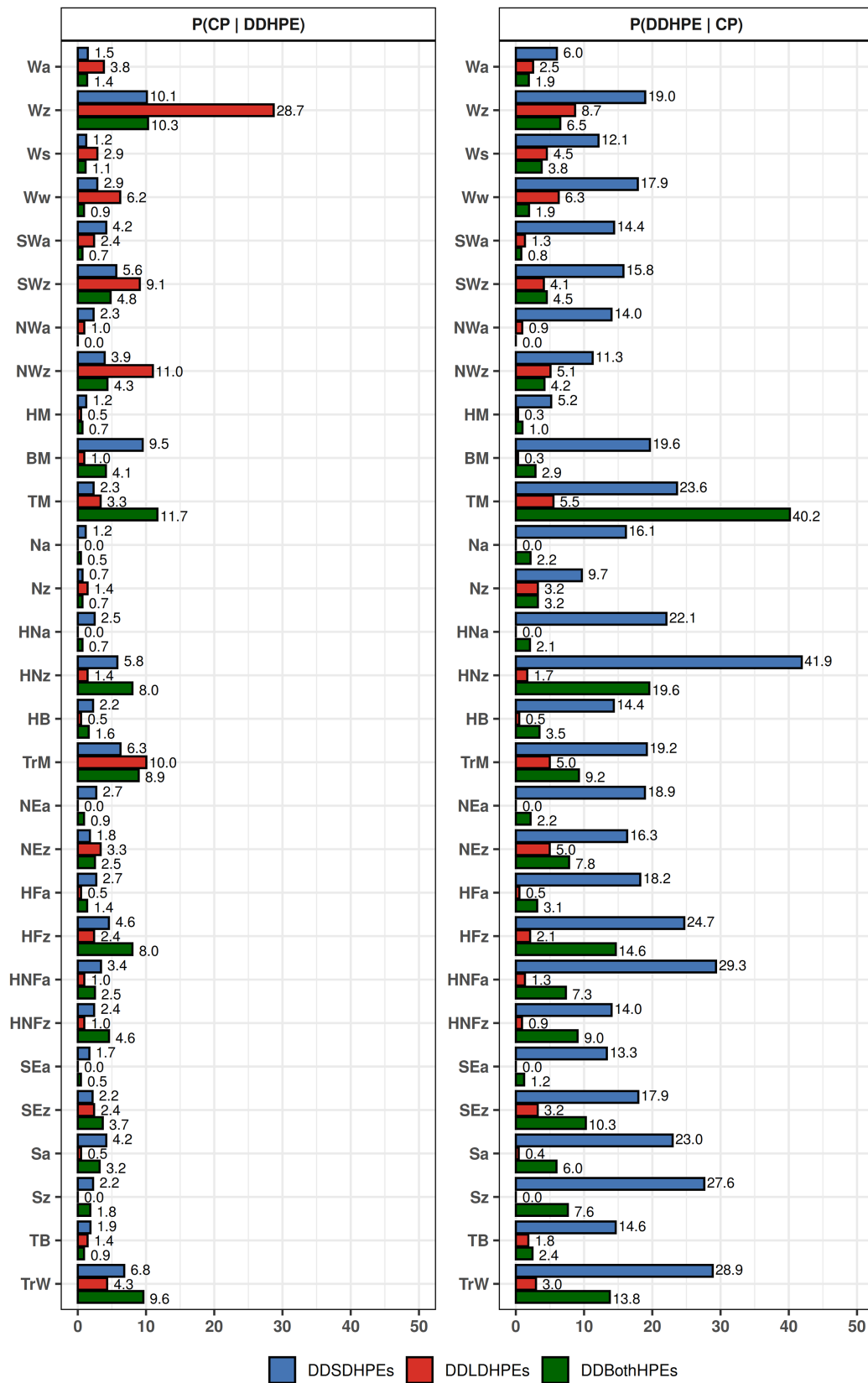


FIGURE 8 The values of $P(CP|DD_{HPE})$ (left column) and $P(DD_{HPE}|CP)$ (right column) for DD_{HPE} s included in CatRaRE T5 for the GWL-REA classification in the years 2001–2020. The colors indicate various types of DD_{HPE} s, while the numbers in each bar represent the values of $P(CP|DD_{HPE})$ (left column) and $P(DD_{HPE}|CP)$ (right column) of the respective circulation pattern marked on the y-axis. Results obtained for DD_{HPE} s included CatRaRE W3 are provided in Figure S2 [Colour figure can be viewed at [wileyonlinelibrary.com](https://onlinelibrary.wiley.com)]

definition, higher for the more often occurring SDHPEs than for LDHPEs. As an example, for DD_{SDHPEs} , there are five cyclonic and three anticyclonic CPs, for which $P(DD_{HPE}|CP)$ values exceed 20%, while for DD_{LDHPEs} , there are four cyclonic CPs, all with airflow from the western or northern sectors, for which $P(DD_{HPE}|CP)$ values exceed 5%. It is of notable interest that $DD_{BothHPEs}$ is very often associated with TM—a cut-off low pressure system located over Central Europe leads in over 40% of its occurrence to the hydrologically dangerous situation of simultaneous developments of SDHPEs and LDHPEs, appearing on the same day in more or less distant locations. In the summer, such situations are frequently linked to the occurrence of low air pressure dominating the upper troposphere and corresponding depression near the ground, which causes an increasingly unstable stratification of the troposphere intensified by the inflow of warm and humid air masses, usually from the Mediterranean region. An example of such a situation is the low-pressure system “Bernd,” which occurred over Central Europe in July 2021 and led to severe precipitation,

flooding, serious infrastructure damages and fatalities (Szymczak et al., 2022). Also at that time, southwestern Germany, Belgium, Luxembourg and the Netherlands experienced a combination of persistent and recurrent heavy rainfall related to the slowly moving near-surface depression intensified by the inflow of warm and humid air masses from the then exceptionally warm Baltic Sea.

Considering $GWL-REA_{GROUPS}$, HPEs included in CatRaRE 5 are more often accompanied by cyclonic than anticyclonic vorticity classes. The cumulative value of $P(CP|DD_{HPE})$ depends, however, strongly on the DD_{HPE} type, ranging for the cyclonic vorticity classes from 61.0% for DD_{SDHPEs} to 89.4% for DD_{LDHPEs} . As illustrated in Figure 9 (left column), the vast majority of DD_{LDHPEs} is accompanied by the three cyclonic situations with maritime circulation forms (ZWm, ZKm and ZGm). These three groups are distinguished according to air mass temperature. Both ZWm and ZGm have a midlatitude Atlantic source of moisture—the warm group (ZWm) is dominated by moist-warm air masses, while the boundary group (ZGm) features quasi-stationary frontal

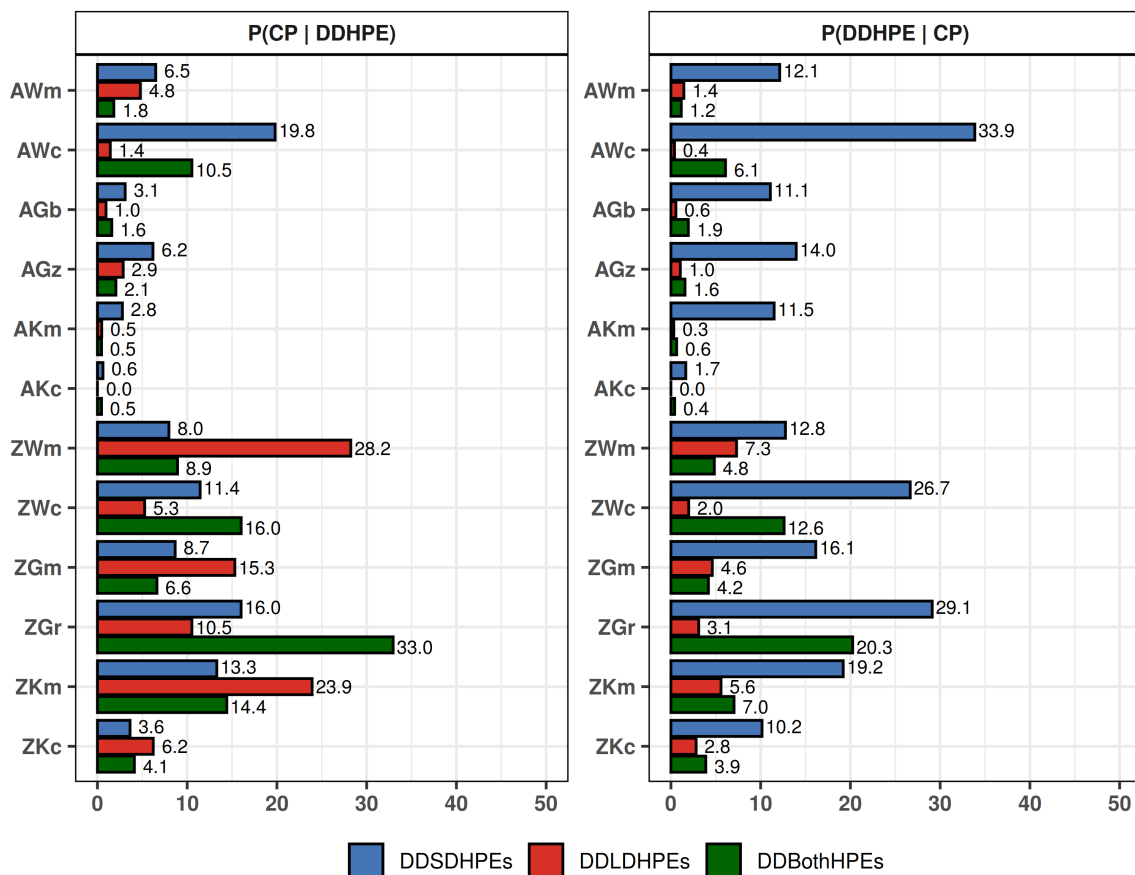


FIGURE 9 The values of $P(CP|DD_{HPE})$ (left column) and $P(DD_{HPE}|CP)$ (right column) for DD_{HPEs} included in CatRaRE T5 for the $GWL-REA_{GROUPS}$ classification in the years 2001–2020. The colors indicate various types of DD_{HPEs} , while the numbers in each bar represent the values of $P(CP|DD_{HPE})$ (left column) and $P(DD_{HPE}|CP)$ (right column) of the respective circulation pattern marked on the y-axis. Results obtained for DD_{HPEs} included CatRaRE W3 are provided in Figure S3 [Colour figure can be viewed at [wileyonlinelibrary.com](https://onlinelibrary.wiley.com)]

systems dividing distinct air masses across Central Europe and situations with returning, warmed polar-maritime air masses, in which the air mass is typically too warm to be included in the cold cyclonic maritime group. This latter group (ZKm) is most often characterized by low-level air flow from the northwest or north underneath an upper trough. While the moisture source here is often from the North Sea or nearby North Atlantic, in some cases very moist Mediterranean air can eventually become entrained into the trough from the east, having spread northwards during the preceding days and leading to prolonged downpours and severe flooding. For DD_{LDHPEs} , the circulation-air mass groups ZWm, ZKm and ZGm reach also the highest values of $P(DD_{HPE}|CP)$ shown in Figure 9 (right column), ranging from 4.6% for ZGm to 7.3% for ZWm. On the other hand, DD_{SDHPEs} are characterized by slightly more equally distributed values of $P(CP|DD_{HPE})$ and $P(DD_{HPE}|CP)$, implying that a wider spectrum of air masses might contribute to SDHPEs development. Moreover, the circulation-air mass group which most often accompanies DD_{SDHPEs} and most often leads to DD_{SDHPEs} consists of anticyclonic situations with warm continental air masses (AWc)—the AWc group not only accompanies every fifth DD_{SDHPEs} , but also every third case of AWc occurrence leads to DD_{SDHPEs} . Relatively high values of $P(CP|DD_{HPE})$ and $P(DD_{HPE}|CP)$ are also achieved by the quite diverse cyclonic situations with a surface frontal trough or with warm advection into a cold air mass (ZGr) and cyclonic situations with warm air masses from the Mediterranean (ZWc). For $DD_{BothHPEs}$, in turn, $P(CP|DD_{HPE})$ and $P(DD_{HPE}|CP)$ reach the highest values for the circulation-air mass group ZGr. This group includes the cut-off low pressure system located over Central Europe, that is, TM in the GWL-REA classification, which has already been identified as the CP most often leading to the simultaneous development of SDHPEs and LDHPEs.

4 | CONCLUSIONS

In this paper, we have provided insight into the spatial and temporal variability of SDHPEs detected by the DWD radar network in Germany from 2001 to 2020 as well as their links to CPs expressed in form of the new numerical method for classifying CPs over Central Europe abbreviated here as GWL-REA. It has been confirmed that SDHPEs, which are defined based on either locally valid precipitation values with a return period of 5 years (CatRaRE T5) or absolute precipitation values equal to DWD Warning Level 3 (CatRaRE W3), constitute common phenomena occurring most frequently in the afternoon hours of the warm season, implying an

essential role of thermal instability for their development. Regardless of the CatRaRE version, the number of SDHPEs is an order of magnitude higher than the number of LDHPEs. Yet over the years, SDHPEs have received substantially less scientific attention than LDHPEs, principally due to the limitations of the measurement systems. These limitations are to a large extent related to the relatively small area of SDHPEs. The median area of SDHPEs ranges from 22 km² (CatRaRE T5) to 24 km² (CatRaRE W3), while the median area of LDHPEs ranges from 175 km² (CatRaRE W3) to 184 km² (CatRaRE T5), as a result of which SDHPEs often cannot be captured by rain gauge stations. This has, in turn, important implications not only for monitoring and understanding of SDHPEs but also for the quality of numerical weather predictions and climate model simulations. For instance, the comprehensive validation of convection-permitting models remains challenging, since the availability of high-resolution radar products is distinctly limited in time and space (Kendon et al., 2021; Prein et al., 2015). Regardless of the catalogue version, SDHPEs are also far less related to topography compared to LDHPEs, which corresponds to the findings of other studies (e.g., Formetta et al., 2022; Marra et al., 2022; Panziera et al., 2016) stating that the spatial variability of HPEs depends on the event duration. For the north-eastern Italian Alps, as an example, Formetta et al. (2022) have identified two modes of orographic relationship: (1) a reverse orographic effect for precipitation with subhourly and hourly durations as well as (2) an orographic enhancement for precipitation with durations of more than 8 h. Whether this relationship also applies to other mountain ranges remains an open issue. Another still open issue is whether local factors, such as urban heat islands or enhanced surface roughness, may induce or modify SDHPEs (Marelle et al., 2020; Xiao et al., 2021).

The results have demonstrated that SDHPEs can be generated by a wide spectrum of circulation conditions, which can be classified into two major groups. The first group constitute cyclonic CPs commonly known as those linked to the development of precipitation and its extremes—good examples are here TrM, TrW, NWz, SWz and Wz, which are associated both with SDHPEs and LDHPEs. Also, TM shows dependencies with both types of HPEs, leading often to hydrologically dangerous situations of the simultaneous occurrence of LDHPEs and SDHPEs, appearing on the same day in more or less distant locations. The second group constitute, in turn, diverse anticyclonic CPs, such as BM, HFa, HNa, HNFa, Sa and SWa. These CPs are associated with the development of SDHPEs, while being at the same time largely irrelevant for LDHPEs. As compared to previous studies, CPs included in the first group have already been

described as those related to the development of HPEs over the various regions of Central Europe (Minářová et al., 2017a, 2017b), while CPs included in the second group have usually been considered far less important for the development of precipitation and its extremes. Based on the manual GWL series, Gerstengarbe and Werner (2005) stated, for instance, that BM, HFa, HNFa, Sa and SWa are characterized in the summer by positive deviations of air temperatures and by negative deviations of precipitation sums. Considering that their study was based on precipitation data gained from rain gauge stations, we can assume that the relatively small-scale convective cells developing under the conditions of high thermal instability were poorly resolved by station-based data, which ultimately led to underestimation of the role of anticyclonic CPs for SDHPEs development.

Furthermore, the application of GWL-REA_{GROUPS} has allowed for an effective and refined identification of circulation-air mass groups associated with the occurrence of various HPEs types. While the vast majority of LDHPEs is related to cyclonic situations with the advection of maritime air masses, SDHPEs may develop under the influence of more diverse circulation-air mass groups, including not only cyclonic but also anticyclonic vorticity classes. The circulation-air mass groups related to SDHPEs development are (1) blocked anticyclonic situations with warm air masses; (2) cyclonic air mass boundary situations with a surface frontal trough or with warm advection into a colder air mass; (3) cyclonic situations under an upper trough and (4) cyclonic situations with warm air masses from the Mediterranean or the Atlantic. Interestingly, these conclusions are very similar for both CatRaRE version (results obtained for CatRaRE W3 are provided in Figures S2 and S3), despite different definitions of HPEs used therein, resulting in diverse spatial distribution of HPEs. From the methodological point of view, GWL-REA_{GROUPS} constitutes a promising tool for assessing meso- and macroscale CPs associated with various meteorological phenomena and can be widely used in follow-up research.

The findings presented in this paper may serve as a baseline for further in-depth studies on the behaviour of SDHPEs under various atmospheric circulation patterns and changing climate, including, for example, studies on projected future intensification of SDHPEs. Such studies are of particular importance for weather forecasting and early warnings, thus serving also as a guidance for investigating (flash)-flood hazards.

AUTHOR CONTRIBUTIONS

Angelika Palarz: Conceptualization; investigation; methodology; software; data curation; validation; visualization; writing – original draft; formal analysis. **Paul James:**

Conceptualization; methodology; investigation; validation; writing – original draft; visualization; formal analysis; data curation. **Thomas Junghänel:** Conceptualization; supervision; project administration; visualization; investigation; writing – original draft; methodology; resources. **Jennifer Ostermüller:** Conceptualization; investigation; visualization; writing – original draft; methodology. **Ewelina Walawender:** Methodology; investigation; writing – original draft; conceptualization; visualization. **Thomas Deutschländer:** Project administration; resources; supervision; funding acquisition; writing – original draft; conceptualization; methodology.

ACKNOWLEDGEMENT

This research and development work by BMDV Network of Experts “Knowledge-Ability-Action” was funded by the Federal Ministry for Digital and Transport (BMDV).



CONFLICT OF INTEREST STATEMENT

The authors declare no conflicts of interest.

DATA AVAILABILITY STATEMENT

The Catalogue of Radar based heavy Rainfall Events (CatRaRE) is openly available in DWD's Open Data Server at: <https://www.dwd.de/DE/leistungen/catrare/catrare.html>, while the “Großwetterlagen for Reanalyses” (GWL REA) are available from the authors upon request.

ORCID

Angelika Palarz  <https://orcid.org/0000-0002-5749-2507>
Ewelina Walawender  <https://orcid.org/0000-0002-0956-4406>

REFERENCES

- Ali, H., Fowler, H.J., Pritchard, D., Lenderink, G. & Blenkinsop, L.E. (2022) Towards quantifying the uncertainty in estimating observed scaling rates. *Geophysical Research Letters*, 49, e2022GL099138. Available from: <https://doi.org/10.1029/2022GL099138>
- Ali, H., Peleg, N. & Fowler, H.J. (2021) Global scaling of rainfall with dewpoint temperature reveals considerable ocean-land difference. *Geophysical Research Letters*, 48, e2021GL093798. Available from: <https://doi.org/10.1029/2021GL093798>
- Arnbjerg-Nielsen, K., Willems, P., Olsson, J., Beecham, S., Pathirana, A., Bülow Gregersen, I. et al. (2013) Impacts of climate change on rainfall extremes and urban drainage systems: a review. *Water Science and Technology*, 68, 16–28. Available from: <https://doi.org/10.2166/wst.2013.251>
- Ban, N., Schmidli, J. & Schär, C. (2015) Heavy precipitation in a changing climate: Does short-term summer precipitation increase faster? *Geophysical Research Letters*, 42, 1165–1172. Available from: <https://doi.org/10.1002/2014GL062588>
- Barton, Y., Sideris, I.V., Raupach, T.H., Gabella, M., Germann, U. & Martius, O. (2020) A multi-year assessment of sub-hourly gridded precipitation for Switzerland based on a blended radar-

- rain-gauge dataset. *International Journal of Climatology*, 40, 5208–5222. Available from: <https://doi.org/10.1002/joc.6514>
- Berg, P., Norin, L. & Olsson, J. (2016) Creation of a high resolution precipitation data set by merging gridded gauge data and radar observations for Sweden. *Journal of Hydrology*, 541, 6–13. Available from: <https://doi.org/10.1016/j.jhydrol.2015.11.031>
- Blenkinsop, S., Fowler, H.J., Barbero, R., Chan, S.C., Guerreiro, S.B., Kendon, E. et al. (2018) The INTENSE project: using observations and models to understand the past, present and future of sub-daily rainfall extremes. *Advances in Science and Research*, 15, 117–126. Available from: <https://doi.org/10.5194/asr-15-117-2018>
- Blížňák, V., Kašpar, M. & Müller, M. (2018) Radar-based summer precipitation climatology of the Czech Republic. *International Journal of Climatology*, 38, 677–691. Available from: <https://doi.org/10.1002/joc.5202>
- Brieber, A. & Hoy, A. (2019) Statistical analysis of very high-resolution precipitation data and relation to atmospheric circulation in Central Germany. *Advances in Science and Research*, 16, 69–73. Available from: <https://doi.org/10.5194/asr-16-69-2019>
- Chan, S.C., Kendon, E.J., Berthou, S., Fossier, G., Lewis, E. & Fowler, H.J. (2020) Europe-wide precipitation projections at convection permitting scale with the Unified Model. *Climate Dynamics*, 55, 409–428. Available from: <https://doi.org/10.1007/s00382-020-05192-8>
- Chen, H. & Sun, J. (2021) Significant increase of the global population exposure to increased precipitation extremes in the future. *Earth's Future*, 9, e2020EF001941. Available from: <https://doi.org/10.1029/2020EF001941>
- Chen, H., Sun, J. & Li, J. (2020) Increased population exposure to precipitation extremes under future warmer climates. *Environmental Research Letters*, 15, 034048. Available from: <https://doi.org/10.1088/1748-9326/ab751f>
- Donat, M.G., Angéllil, O. & Ukkola, A.M. (2019) Intensification of precipitation extremes in the world's humid and water-limited regions. *Environmental Research Letters*, 14, 065003. Available from: <https://doi.org/10.1088/1748-9326/ab1c8e>
- Dong, X., Zhang, S., Zhou, J., Cao, J., Jiao, L., Zhang, Z. et al. (2019) Magnitude and frequency of temperature and precipitation extremes and the associated atmospheric circulation patterns in the Yellow River Basin (1960–2017), China. *Water*, 11, 2334. Available from: <https://doi.org/10.3390/w11112334>
- Drücke, J., Borsche, M., James, P., Kaspar, F., Pfeifroth, U., Ahrens, B. et al. (2021) Climatological analysis of solar and wind energy in Germany using the Grosswetterlagen classification. *Renewable Energy*, 164, 1254–1266. Available from: <https://doi.org/10.1016/j.renene.2020.10.102>
- Fairman, J.G., Jr., Schultz, D.M., Kirshbaum, D.J., Gray, S.L. & Barrett, A.I. (2015) A radar-based rainfall climatology of Great Britain and Ireland. *Weather*, 70, 153–158. Available from: <https://doi.org/10.1002/wea.2486>
- Fairman, J.G., Jr., Schultz, D.M., Kirshbaum, D.J., Gray, S.L. & Barrett, A.I. (2017) Climatology of size, shape, and intensity of precipitation features over Great Britain and Ireland. *Journal of Hydrometeorology*, 18, 1595–1615. Available from: <https://doi.org/10.1175/JHM-D-16-0222.1>
- Fernández-Montes, S., Seubert, S., Rodrigo, F.S., Álvarez, D.R., Hertig, E., Esteban, P. et al. (2014) Circulation types and extreme precipitation days in the Iberian Peninsula in the transition seasons: spatial links and temporal changes. *Atmospheric Research*, 138, 41–58. Available from: <https://doi.org/10.1016/j.atmosres.2013.10.018>
- Formetta, G., Marra, F., Dallan, E., Zaramella, M. & Borga, M. (2022) Differential orographic impact on sub-hourly, hourly, and daily extreme precipitation. *Advances in Water Resources*, 159, 104085. Available from: <https://doi.org/10.1016/j.advwatres.2021.104085>
- Fowler, H.J., Ali, H., Allan, R.P., Ban, N., Barbero, R., Berg, P. et al. (2021) Towards advancing scientific knowledge of climate change impacts on short-duration rainfall extremes. *Philosophical Transactions of the Royal Society*, 379, 20190542. Available from: <https://doi.org/10.1098/rsta.2019.0542>
- Gerstengarbe, F.W. & Werner, P.C. (2005) *Katalog der Grosswetterlagen Europas (1881–2004) nach Paul Hess und Helmut Brezowsky*. Potsdam, Germany: Potsdam Institute für Klimafolgenforschung (in German).
- Hersbach, H., Bell, B., Berrisford, P., Hirahara, S., Horányi, A., Muñoz-Sabater, J. et al. (2020) The ERA5 global reanalysis. *Quarterly Journal of the Royal Meteorological Society*, 146, 1999–2049. Available from: <https://doi.org/10.1002/qj.3803>
- Hess, P. & Brezowsky, H. (1952) *Katalog der Grosswetterlagen Europas*, Vol. 33. Bad Kissingen, Germany: Berichte des Deutschen Wetterdienstes in der US-Zone (in German).
- Hoy, A., Schucknecht, A., Sepp, M. & Matschullat, J. (2014) Large-scale synoptic types and their impact on European precipitation. *Theoretical and Applied Climatology*, 116, 19–35. Available from: <https://doi.org/10.1007/s00704-013-0897-x>
- IPCC. (2012) *Managing the risks of extreme events and disasters to advance climate change adaptation special report of the Intergovernmental Panel on Climate Change*. Cambridge: Cambridge University Press.
- IPCC. (2023) *Climate change 2021: the physical science basis. Contribution of Working Group I to the sixth assessment report of the Intergovernmental Panel on climate change*. Cambridge: Cambridge University Press.
- Iqbal, Z., Shahid, S., Ahmed, K., Ismail, T. & Nawaz, N. (2019) Spatial distribution of the trends in precipitation and precipitation extremes in the sub-Himalayan region of Pakistan. *Theoretical and Applied Climatology*, 137, 2755–2769. Available from: <https://doi.org/10.1007/s00704-019-02773-4>
- Irannezhad, M., Chen, D., Kløve, B. & Moradkhani, H. (2017) Analysing the variability and trends of precipitation extremes in Finland and their connection to atmospheric circulation patterns. *International Journal of Climatology*, 37, 1053–1066. Available from: <https://doi.org/10.1002/joc.5059>
- Jaagus, J., Briede, A., Rimkus, E. & Remm, K. (2010) Precipitation pattern in the Baltic countries under the influence of large-scale atmospheric circulation and local landscape factors. *International Journal of Climatology*, 30, 705–720. Available from: <https://doi.org/10.1002/joc.1929>
- James, P. (2007) An objective classification method for Hess and Brezowsky Grosswetterlagen over Europe. *Theoretical and Applied Climatology*, 88, 17–42. Available from: <https://doi.org/10.1007/s00704-006-0239-3>
- Jenkinson, A.F. & Collison, F.P. (1977) *An initial climatology of gales over the North Sea*. Synoptic climatol branch memorandum 62, p. 18.
- Kang, N., Kim, S., Kim, Y., Noh, H., Hong, S.J. & Kim, H.S. (2016) Urban drainage system improvement for climate change

- adaptation. *Water*, 8, 268. Available from: <https://doi.org/10.3390/w8070268>
- Kendon, E.J., Blenkinsop, S. & Fowler, H.J. (2018) When will we detect changes in short-duration precipitation extremes? *Journal of Climate*, 31, 2945–2964. Available from: <https://doi.org/10.1175/JCLI-D-17-0435.1>
- Kendon, E.J., Prein, A.F., Senior, C.A. & Stirling, A. (2021) Challenges and outlook for convection-permitting climate modelling. *Philosophical Transactions of the Royal Society A*, 379, 20190547. Available from: <https://doi.org/10.1098/rsta.2019.0547>
- Kenyon, J. & Hegerl, G.C. (2010) Influence of modes of climate variability on global precipitation extremes. *Journal of Climate*, 23, 6248–6262. Available from: <https://doi.org/10.1175/2010JCLI3617.1>
- Kourtis, I.M. & Tsihrintzis, V.A. (2021) Adaptation of urban drainage networks to climate change: a review. *Science of the Total Environment*, 771, 145431. Available from: <https://doi.org/10.1016/j.scitotenv.2021.145431>
- Kreklow, J., Tetzlaff, B., Burkhard, B. & Kuhnt, G. (2020) Radar-based precipitation climatology in Germany—developments, uncertainties and potentials. *Atmosphere*, 11, 217. Available from: <https://doi.org/10.3390/atmos11020217>
- Lenderink, G. & Meijgaard, E.V. (2008) Increase in hourly precipitation extremes beyond expectations from temperature changes. *Nature Geoscience*, 1(8), 511–514. Available from: <https://doi.org/10.1038/ngeo262>
- Lengfeld, K., Kirstetter, P.E., Fowler, H.J., Yu, J., Becker, A., Flamig, Z. et al. (2020) Use of radar data for characterizing extreme precipitation at fine scales and short durations. *Environmental Research Letters*, 15, 085003. Available from: <https://doi.org/10.1088/1748-9326/ab98b4>
- Lengfeld, K., Walawender, E., Winterrath, T. & Becker, A. (2021a) CatRaRE: a catalogue of radar-based heavy rainfall events in Germany derived from 20 years of data. *Meteorologische Zeitschrift*, 6, 469–487. Available from: <https://doi.org/10.1127/metz/2021/1088>
- Lengfeld, K., Walawender, E., Winterrath, T., Weigl, E. & Becker, A. (2021b) Heavy precipitation events version 2021.01 exceeding DWD warning level 3 for severe weather based on RADKLIM-RW version 2017.002. https://doi.org/10.5676/DWD/CatRaRE_W3_Eta_v2021.01CatRaREW3
- Lengfeld, K., Walawender, E., Winterrath, T., Weigl, E. & Becker, A. (2021c) Heavy precipitation events version 2021.01 exceeding return period of 5 years from RADKLIM-RW version 2017.002. https://doi.org/10.5676/DWD/CatRaRE_T5_Eta_v2021.01
- Lengfeld, K., Winterrath, T., Junghänel, T., Hafer, M. & Becker, A. (2019) Characteristic spatial extent of hourly and daily precipitation events in Germany derived from 16 years of radar data. *Meteorologische Zeitschrift*, 28, 363–378. Available from: <https://doi.org/10.1127/metz/2019/0964>
- Lewis, E., Fowler, H., Alexander, L., Dunn, R., McClean, F., Barbero, R. et al. (2019) GSDR: a global sub-daily rainfall dataset. *Journal of Climate*, 32, 4715–4729. Available from: <https://doi.org/10.1175/JCLI-D-18-0143.1>
- Li, H., Chen, H., Wang, H. & Yu, E. (2018a) Future precipitation changes over China under 1.5°C and 2.0°C global warming targets by using CORDEX regional climate models. *Science of the Total Environment*, 640, 543–554. Available from: <https://doi.org/10.1016/j.scitotenv.2018.05.324>
- Li, X., Xuan, W. & Babovic, V. (2018b) Analysis of variability and trends of precipitation extremes in Singapore during 1980–2013. *International Journal of Climatology*, 38, 125–141. Available from: <https://doi.org/10.1002/joc.5165>
- Liu, Y., Chen, J., Pan, T., Liu, Y., Zhang, Y., Ge, Q. et al. (2020) Global socioeconomic risk of precipitation extremes under climate change. *Earth's Future*, 8, e2019EF001331. Available from: <https://doi.org/10.1029/2019EF001331>
- Loriaux, J.M., Lenderink, G., De Roode, S.R. & Siebesma, A.P. (2013) Understanding convective extreme precipitation scaling using observations and an entraining plume model. *Journal of the Atmospheric Sciences*, 70, 3641–3655. Available from: <https://doi.org/10.1175/JAS-D-12-0317.1>
- Luino, F., De Graff, J., Roccati, A., Biddoccu, M., Cirio, C.G., Faccini, F. et al. (2019) Eighty years of data collected for the determination of rainfall threshold triggering shallow landslides and mud-debris flows in the Alps. *Water*, 12, 133. Available from: <https://doi.org/10.3390/w12010133>
- Lupikasza, E. (2010) Relationships between occurrence of high precipitation and atmospheric circulation in Poland using different classifications of circulation types. *Physics and Chemistry of the Earth*, 35, 448–455. Available from: <https://doi.org/10.1016/j.pce.2009.11.012>
- Marelle, L., Myhre, G., Steensen, B.M., Hodnebrog, Ø., Alterskjær, K. & Sillmann, J. (2020) Urbanization in megacities increases the frequency of extreme precipitation events far more than their intensity. *Environmental Research Letters*, 15, 124072. Available from: <https://doi.org/10.1088/1748-9326/abcc8f>
- Marra, F., Armon, M. & Morin, E. (2022) Coastal and orographic effects on extreme precipitation revealed by weather radar observations. *Hydrology and Earth System Sciences*, 26, 1439–1458. Available from: <https://doi.org/10.5194/hess-26-1439-2022>
- Merino, A., Fernández-Vaquero, M., López, L., Fernández-González, S., Hermida, L., Sánchez, J.L. et al. (2016) Large-scale patterns of daily precipitation extremes on the Iberian Peninsula. *International Journal of Climatology*, 36, 3873–3891. Available from: <https://doi.org/10.1002/joc.4601>
- Meynen, E. & Schmithausen, J. (1959) Handbuch der naturräumlichen Gliederung Deutschlands. Teil 9 in Veröffentlichung der Bundesanstalt für Landeskunde und des Deutschen Instituts für Landeskunde–Verlag der Bundesanstalt. für Landeskunde (in German).
- Mika, J., Károssy, C. & Lakatos, L. (2021) Variations in the Peczely macro-synoptic types (1881–2020) with attention to weather extremes in the Pannonian Basin. *Atmosphere*, 12, 1071. Available from: <https://doi.org/10.3390/atmos12081071>
- Minářová, J., Müller, M., Clappier, A., Hänsel, S., Hoy, A., Matschullat, J. et al. (2017b) Duration, rarity, affected area, and weather types associated with extreme precipitation in the Ore Mountains (Erzgebirge) region, Central Europe. *International Journal of Climatology*, 37, 4463–4477. Available from: <https://doi.org/10.1002/joc.5100>
- Minářová, J., Müller, M., Clappier, A. & Kašpar, M. (2017a) Characteristics of extreme precipitation in the Vosges Mountains region (North-Eastern France). *International Journal of Climatology*, 37, 4529–4542. Available from: <https://doi.org/10.1002/joc.5102>
- Müller, M. & Kaspar, M. (2014) Event-adjusted evaluation of weather and climate extremes. *Natural Hazards and Earth System Sciences*, 14, 473–483. Available from: <https://doi.org/10.5194/nhess-14-473-2014>

- Nguyen, P., Thorstensen, A., Sorooshian, S., Hsu, K., Agha Kouchak, A., Sanders, B. et al. (2016) A high resolution coupled hydrologic–hydraulic model (HiResFlood-UCI) for flash flood modeling. *Journal of Hydrology*, 541, 401–420. Available from: <https://doi.org/10.1016/j.jhydrol.2015.10.047>
- Oh, S. & Sushama, L. (2020) Short-duration precipitation extremes over Canada in a warmer climate. *Climate Dynamics*, 54, 2493–2509. Available from: <https://doi.org/10.1007/s00382-020-05126-4>
- Orlanski, I. (1975) A rational subdivision of scales for atmospheric processes. *Bulletin of the American Meteorological Society*, 56, 527–530.
- Panziera, L., Gabella, M., Germann, U. & Martius, O. (2018) A 12-year radar-based climatology of daily and sub-daily extreme precipitation over the Swiss Alps. *International Journal of Climatology*, 38, 3749–3769. Available from: <https://doi.org/10.1002/joc.5528>
- Panziera, L., Gabella, M., Zanini, S., Hering, A., Germann, U. & Berne, A. (2016) A radar-based regional extreme rainfall analysis to derive the thresholds for a novel automatic alert system in Switzerland. *Hydrology and Earth System Sciences*, 20, 2317–2332. Available from: <https://doi.org/10.5194/hess-20-2317-2016>
- Paulat, M., Frei, C., Hagen, M. & Wernli, H. (2008) A gridded dataset of hourly precipitation in Germany: its construction, climatology and application. *Meteorologische Zeitschrift*, 17, 719–732. Available from: <https://doi.org/10.1127/0941-2948/2008/0332>
- Powell, E.J. & Keim, B. (2015) Trends in daily temperature and precipitation extremes for the southeastern United States: 1948–2012. *Journal of Climate*, 28, 1592–1612. Available from: <https://doi.org/10.1175/JCLI-D-14-00410.1>
- Prein, A.F., Langhans, W., Fosser, G., Ferrone, A., Ban, N., Goergen, K. et al. (2015) A review on regional convection-permitting climate modeling: demonstrations, prospects, and challenges. *Reviews of Geophysics*, 53, 323–361. Available from: <https://doi.org/10.1002/2014RG000475po>
- Rajczak, J. & Schär, C. (2017) Projections of future precipitation extremes over Europe: a multimodel assessment of climate simulations. *Journal of Geophysical Research: Atmospheres*, 122, 10773–10800. Available from: <https://doi.org/10.1002/2017JD027176>
- Řehoř, J., Brázdil, R., Lhotka, O., Trnka, M., Balek, J., Štěpánek, P. et al. (2021) Precipitation in The Czech Republic in light of subjective and objective classifications of circulation types. *Atmosphere*, 12, 1536. Available from: <https://doi.org/10.3390/atmos12111536>
- Rimbu, N., Stefan, S., Busuioc, A. & Georgescu, F. (2016) Links between blocking circulation and precipitation extremes over Romania in summer. *International Journal of Climatology*, 36, 369–376. Available from: <https://doi.org/10.1002/joc.4353>
- Romang, H., Zappa, M., Hilker, N., Gerber, M., Dufour, F., Frede, V. et al. (2011) IFKIS-Hydro: an early warning and information system for floods and debris flows. *Natural Hazards*, 56, 509–527. Available from: <https://doi.org/10.1007/s11069-010-9507-8>
- Ryan, C., Curley, M., Walsh, S. & Murphy, C. (2021) Long-term trends in extreme precipitation indices in Ireland. *International Journal of Climatology*, 42, 4040–4061. Available from: <https://doi.org/10.1002/joc.7475>
- Šálek, M., Brezková, L. & Novák, P. (2006) The use of radar in hydrological modeling in The Czech Republic—case studies of flash floods. *Natural Hazards and Earth System Sciences*, 6, 229–236. Available from: <https://doi.org/10.5194/nhess-6-229-2006>
- Saltikoff, E., Friedrich, K., Soderholm, J., Lengfeld, K., Nelson, B., Becker, A. et al. (2019) An overview of using weather radar for climatological studies: successes, challenges, and potential. *Bulletin of the American Meteorological Society*, 100, 1739–1752. Available from: <https://doi.org/10.1175/BAMS-D-18-0166.1>
- Spyrou, C., Varlas, G., Pappa, A., Mentzafou, A., Katsafados, P., Papadopoulos, A. et al. (2020) Implementation of a nowcasting hydrometeorological system for studying flash flood events: the case of Mandra, Greece. *Remote Sensing*, 12, 2784. Available from: <https://doi.org/10.3390/rs12172784>
- Supari, T.F., Junenga, L., Cruz, F., Chung, J.X., Ngai, S.T., Salimuna, E. et al. (2020) Multi-model projections of precipitation extremes in Southeast Asia based on CORDEX-Southeast Asia simulations. *Environmental Research*, 184, 109350. Available from: <https://doi.org/10.1016/j.envres.2020.109350>
- Szymczak, S., Backendorf, F., Bott, F., Fricke, K., Junghänel, T. & Walawender, E. (2022) Impacts of heavy and persistent precipitation on railroad infrastructure in July 2021: a case study from the Ahr Valley, Rhineland-Palatinate, Germany. *Atmosphere*, 13, 1118. Available from: <https://doi.org/10.3390/atmos13071118>
- Tan, X., Gan, T.Y., Chen, S., Horton, D.E., Chen, X., Liu, B. et al. (2019) Trends in persistent seasonal-scale atmospheric circulation patterns responsible for seasonal precipitation totals and occurrences of precipitation extremes over Canada. *Journal of Climate*, 32, 7105–7126. Available from: <https://doi.org/10.1175/JCLI-D-18-0408.1>
- Tapiador, F.J., Turk, F.J., Petersen, W., Hou, A.Y., Garcia-Ortega, E., Machado, L.A.T. et al. (2012) Global precipitation measurement: methods, datasets and applications. *Atmospheric Research*, 104, 70–97. Available from: <https://doi.org/10.1016/j.atmosres.2011.10.021>
- Twardosz, R. & Niedźwiedz, T. (2001) Influence of synoptic situations on the precipitation in Kraków (Poland). *International Journal of Climatology*, 21, 467–481.
- Ullah, W., Wang, G., Lou, D., Ullah, S., Bhatti, A.S., Ullah, S. et al. (2021) Large-scale atmospheric circulation patterns associated with extreme monsoon precipitation in Pakistan during 1981–2018. *Atmospheric Research*, 253, 105489. Available from: <https://doi.org/10.1016/j.atmosres.2021.105489>
- Ustrnul, Z. & Czekierda, D. (2001) Circulation background of the atmospheric precipitation in Central Europe (based on the Polish example). *Meteorologische Zeitschrift*, 10, 103–112. Available from: <https://doi.org/10.1127/0941-2948/2001/0010-0103>
- Wapler, K. & James, P. (2015) Thunderstorm occurrence and characteristics in Central Europe under different synoptic conditions. *Atmospheric Research*, 158, 231–244. Available from: <https://doi.org/10.1016/j.atmosres.2014.07.011>
- Winterrath, T., Brendel, C., Hafer, M., Junghänel, T., Klameth, A., Lengfeld, K. et al. (2018) RADKLIM version 2017.002: reprocessed gauge-adjusted radar data, one-hour precipitation sums (RW). https://doi.org/10.5676/DWD/RADKLIM_RW_V2017.002
- Xiao, F., Zhu, B. & Zhu, T. (2021) Inconsistent urbanization effects on summer precipitation over the typical climate regions in

- central and eastern China. *Theoretical and Applied Climatology*, 143, 73–85. Available from: <https://doi.org/10.1007/s00704-020-03404-z>
- Yang, Z., Wang, L., Qiao, J., Uchimura, T. & Wang, L. (2020) Application and verification of a multivariate real-time early warning method for rainfall-induced landslides: implication for evolution of landslide-generated debris flows. *Landslides*, 17, 2409–2419. Available from: <https://doi.org/10.1007/s10346-020-01402-w>
- Yun, Y., Liu, C., Luo, Y., Liang, X., Huang, L., Chen, F. et al. (2020) Convection-permitting regional climate simulation of warm-season precipitation over eastern China. *Climate Dynamics*, 54, 1469–1489. Available from: <https://doi.org/10.1007/s00382-019-05070-y>
- Zhai, X., Guo, L., Liu, R. & Zhang, Y. (2018) Rainfall threshold determination for flash flood warning in mountainous catchments with consideration of antecedent soil moisture and rainfall pattern. *Natural Hazards*, 94, 605–625. Available from: <https://doi.org/10.1007/s11069-018-3404-y>
- Zhou, Q. (2014) A review of sustainable urban drainage systems considering the climate change and urbanization impacts. *Water*, 6, 976–992. Available from: <https://doi.org/10.3390/w6040976>

SUPPORTING INFORMATION

Additional supporting information can be found online in the Supporting Information section at the end of this article.

How to cite this article: Palarz, A., James, P., Junghänel, T., Ostermöller, J., Walawender, E., & Deutschländer, T. (2024). Radar-based heavy precipitation events in Germany and associated circulation patterns. *International Journal of Climatology*, 44(1), 196–216. <https://doi.org/10.1002/joc.8323>